

## Time domain intrusive probabilistic seismic risk analysis of nonlinear shear frame structure

Hexiang Wang<sup>a</sup>, Fangbo Wang<sup>b</sup>, Han Yang<sup>a</sup>, Yuan Feng<sup>a</sup>, Jeff Bayless<sup>a</sup>,  
Norman A. Abrahamson<sup>a</sup>, Boris Jeremić<sup>a,c,\*</sup>

<sup>a</sup> Department of Civil and Environmental Engineering, University of California, Davis, CA, USA

<sup>b</sup> School of Civil Engineering, Tianjin University, Tianjin, China

<sup>c</sup> Earth and Environmental Sciences Area, Lawrence Berkeley National Laboratory, Berkeley, CA, USA

### ARTICLE INFO

Presented new framework avoids the drawbacks of choosing and using intensity measure (s). All the seismic motion characteristics and their uncertainties, for example, uncertain peak ground acceleration (PGA), spectrum acceleration ( $S_a$ ) and others, are captured by random process motions and directly propagated into uncertain structural system. Development of ground motion prediction equations (GMPEs) for potentially new intensity measures (IMs) (e.g., Arias intensity or cumulative absolute velocity) and repetitive Monte Carlo fragility simulations are circumvented. Though most of current seismic risk analyses are performed for damage measure defined on single engineering demand parameter, presented framework can also handle joint engineering demand parameters/failure criteria without much additional effort. It is found that, for different damage measure defined on joint engineering demand parameters, corresponding seismic risk significantly varies and is rather different from the risk value for single engineering demand parameter. Therefore, considering damage measure based on joint engineering demand parameters can be of great interest in seismic risk analysis. Future work will focus on accuracy and efficiency comparison between the proposed framework and existing intensity measure based, non-intrusive seismic risk analysis and also applying the proposed framework to more realistic engineering structures.

### Keywords:

Probabilistic seismic risk analysis  
Stochastic ground motion  
Stochastic elastoplastic FEM

### ABSTRACT

Presented is a time domain intrusive framework for probabilistic seismic risk analysis. Seismic source characterization is mathematically formulated. Methodology for simulating non-stationary seismic motions for given source, path and site is proposed. Both uncertain motions and uncertain structural parameters are characterized as random process/field and represented with Hermite polynomial chaos. Intrusive modeling of Armstrong-Fredrick kinematic hardening based on Hermite polynomial chaos is formulated and incorporated into Galerkin stochastic elastic-plastic FEM. Time-evolving probabilistic structural response is solved through developed stochastic elastic-plastic FEM. Following that, formulation for seismic risk analysis is derived. The framework is illustrated by seismic risk analysis of an eight-story shear frame structure. Uncertainties are propagated from earthquake source into uncertain structural system. Difficulties of choosing intensity measure in the conventional framework are avoided since all the uncertainties and important characteristics (e.g., spectrum acceleration  $S_a$  and peak ground acceleration  $PGA$ ) of seismic motions are directly carried by the random process excitations in time domain. Stochastic dynamic equations are solved in an intrusive way, circumventing non-intrusive Monte Carlo simulations.

\* Corresponding author. Department of Civil and Environmental Engineering, University of California, Davis, CA, USA.

E-mail address: [jeremic@ucdavis.edu](mailto:jeremic@ucdavis.edu) (B. Jeremić).

<https://doi.org/10.1016/j.soildyn.2020.106201>

Received 22 October 2019; Received in revised form 20 February 2020; Accepted 24 April 2020

Available online 6 June 2020

0267-7261/© 2020 Elsevier Ltd. All rights reserved.

Time domain  
Fourier amplitude spectra

## 1. Introduction

Performance-based Earthquake Engineering (PBEE) [1] has been a successful framework that allows for objective and quantitative decision-making through seismic risk analyses.

Equation (1) demonstrates state of the art methodology of seismic risk analysis:

$$\lambda(EDP > z) = \int \underbrace{\frac{d\lambda(IM > x)}{dx}}_{\text{PSHA}} \underbrace{G(EDP > z | IM = x)}_{\text{fragility}} dx \quad (1)$$

where  $\lambda(EDP > z)$  is the annual rate of engineering demand parameter (EDP, i.e., performance target) exceeding specific level  $z$ . EDP hazard is computed as convolution of probabilistic seismic hazard analysis (PSHA) results and structural fragility with respect to intensity measure (IM) of ground shaking. PSHA, usually done by engineering seismologist, estimates exceedance rate of intensity measure  $\lambda(IM > x)$  considering all possible faults and scenarios near the engineering site. Structural fragility  $G(EDP > z | IM = x)$  defines the exceeding probability of EDP given ground motion with particular IM level  $x$ . With properly defined damage measure (DM) as a function of EDP(s), seismic risk of damage state can be calculated.

The choice of IM is crucial in seismic risk analysis, as it serves as proxy of damaging ground motions and all the uncertainties in ground motion are assumed could be represented by the variability of IM. Spectral acceleration  $Sa(T_0)$  is commonly adopted as IM for building structures. Many ground motion predictions equations (GMPEs) are developed to quantify the median and aleatory variability of  $Sa(T_0)$  [2]. However, the problem is that the scalar spectral acceleration cannot fully describe the influence of ground-motion variability upon engineering objects. Stafford and Bommer [3] investigated different intensity measures and found that they are generally not strongly correlated, which indicates that knowledge of just one IM distribution is not sufficient to describe any of the other ground-motion characteristics.

In addition,  $Sa(T_0)$  as IM for surface building structures, is based on frequency domain, linear dynamic analysis of single degree of freedom system. When nonlinear inelastic and/or higher mode response is expected, use of  $Sa(T_0)$  is not appropriate. Nonlinear response history analysis (RHA) with spectrum-matched ground motion is found to give un-conservatively biased estimates [4,5]. Grigoriu [6] showed that generally  $Sa(T_0)$  is weakly dependent with engineering demand parameters for realistic structures and fragilities defined as functions of  $Sa(T_0)$  have large uncertainties and of limited practical use. Furthermore, for many other engineering objects (e.g., dams, deeply embedded structures, etc.), it is very difficult to find a proper IM in engineering practices. For example, choice of IM among peak ground acceleration (PGA), peak ground velocity (PGV), Arias intensity (AI) and cumulative absolute velocity (CAV) has been contentiously argued for deformation analysis of dam embankment [7]. Though Vector-valued PSHA [8] was put forward to mitigate this issue, it is rarely performed in practices. The difficulty lies in fragility computation. The fragility becomes a function of vector IMs (e.g., a fragility surface for two IMs), which requires a large number of structural analyses to be quantified. Properly choosing multiple IMs is also a problem. Many times, even if proper IMs, such as AI and CAV, are identified, additional efforts are still needed to develop GMPE for these IMs and their correlation.

An effective solution to the aforementioned problems would be to remove intensity measure (IM) as an intermediate proxy from risk calculation. With this in mind, a time domain intrusive framework for probabilistic seismic risk analysis is developed and described here. The

framework is based on the progress of Fourier amplitude spectrum (FAS) modeling of seismic motions over last several decades [9–12]. Recent advances in inter-frequency correlation of FAS [13,14] and Fourier phase derivative modeling [15] are also taken into account. Uncertain motions are simulated from stochastic FAS and Fourier phase spectrum (FPS), and are modeled as non-stationary random process in time domain. With the proposed framework, engineering seismologists do not need to interpret/simplify ground motion into IM(s). Correspondingly, structural engineers do not need to compute fragility curve based on IM. Instead, all the important characteristics and uncertainties in seismic motions are captured through the random process and propagated into uncertain engineering system with direct ‘‘communication’’ between engineering seismologists and structural engineers.

Another feature of the proposed framework is the circumvention of Monte Carlo (MC) simulation. MC approach is non-intrusive in the sense that no modifications to the underlying deterministic solver are required. The state of probabilistic space is characterized by large, statistically significant number of deterministic samplings of system random parameters. In conventional seismic risk analysis, structural fragility curve is developed by incremental dynamic analysis (IDA) [16]. IDA, though theoretically straightforward, is numerically demanding because of the slow convergence rate that is inherent in MC approach. Hundreds of structural analysis need to be performed with deterministic sampling of uncertain material properties and uncertain ground excitations at different IM levels. The same issue of MC approach also limits the application of physics-based seismic waveform modeling techniques [17,18] into hazard/risk analysis. Millions of MC earthquake scenarios over regional geology have to be simulated using deterministic wave propagation programs, such as CyberShake [19] considering uncertain kinematic sources, crustal geology and site conditions. Maechling et al. [18] estimated that ‘‘it would require 300 million CPU-hours and well over 100 years to complete all the simulations needed to calculate a PSHA hazard curve’’.

To avoid non-intrusive MC simulation, Galerkin stochastic elastic-plastic finite element method (SEPFEM) has been developed within the authors’ research group over the years [20–25]. Galerkin SEPFEM is an intrusive approach, requiring new developments based on variational formulation of the underlying stochastic partial differential equations (SPDE). Using appropriate choice of orthogonal polynomial chaos basis, intrusive Galerkin SEPFEM guarantees optimal convergence rates, and is more efficient than non-intrusive MC approach [26,27]. Both random field structural parameters and random process seismic motions are represented by Hermite polynomial chaos (PC) [28] with correlation structure characterized by Karhunen-Loève (KL) expansion [29]. Using Galerkin SEPFEM, probabilistic dynamic response of uncertain structural system driven by uncertain seismic motions is represented by unknown PC coefficients. Deterministic linear system equations of these unknown temporal-spatial PC coefficients, equivalent to the original stochastic PDE, are derived from Galerkin projection technique in weak sense. Seismic risk is then computed from probabilistic dynamic structural response.

The organization of this paper is as follows: The proposed time domain intrusive framework for probabilistic seismic risk analysis is formulated in section 2. Next, the proposed methodology is illustrated by a numerical example in section 3 with conclusions drawn in section 4.

## 2. Time domain intrusive framework for seismic risk analysis

The proposed framework consists of four components, as shown in Fig. 1: seismic source characterization (SSC), stochastic ground motion modeling, stochastic finite element analysis and seismic risk

computation.

In the first step, SSC quantifies the uncertainty in earthquake scenarios so that the probabilistic scenario space  $\lambda(M, R, \Theta)$  for a given engineering site can be discretized into  $N$  mutually exclusive events as follows:

$$\lambda(M, R, \Theta) = \cup_{i=1}^N \lambda_i(M_i, R_i, \Theta_i) \quad (2)$$

where  $\lambda(\cdot)$  is the annual occurrence rate,  $M$  is the magnitude and  $R$  is the distance metric, which could be either rupture distance  $R_{rup}$ , hypocenter distance  $R_{hyp}$ , or Joyner-Boore distance  $R_{jb}$ .  $\Theta$  denotes any other scenario metrics that are required for stochastic ground motion modeling, for example, style of fault, hanging wall identifier, etc.  $N$  is the total number of seismic scenarios considering all the active faults in the region. Basic relations for seismic source characterization are formulated in Section 2.1.

For each scenario event  $S_i(M_i, R_i, \Theta_i)$ , section 2.2 presents the procedure to simulate time domain uncertain motions from stochastic FAS and FPS using inverse Fourier transform. The simulated ground motion population for event  $S_i$  is denoted as  $\{\Gamma_i\}$ .

At the third step, both uncertain motions and uncertain structural parameters are represented by Hermite PC-KL expansion as formulated in section 2.3. Two choices are provided here (1) Random process characterization (i.e., PC-KL expansion): is performed for each individual motion population  $\{\Gamma_i\}$  and conduct further Galerkin stochastic FEM analysis for each scenario  $S_i$ . (2) Seismic motion population from different scenarios is first combined as an ensemble population  $\{\Gamma\}$  following Equation (3):

$$\{\Gamma\} = \cup_{i=1}^N \{w_i \otimes \Gamma_i\} \quad (3)$$

with

$$w_i = \frac{\lambda_i}{\sum_{i=1}^N \lambda_i} \quad (4)$$

where  $\cup_{i=1}^N \{w_i \otimes \Gamma_i\}$  denotes the weighted combination of population  $\{\Gamma_i\}$  with weight  $w_i$  defined as Equation (4). The annual occurrence rate of the ensemble population  $\{\Gamma\}$  is  $\bar{\lambda} = \sum_{i=1}^N \lambda_i$ . The weighted combination can be performed by aggregating individual population  $\{\Gamma_i\}$  of different size  $n_i$ ,  $i = 1, 2, \dots, N$  such that  $n_i$  is proportional to  $w_i$ , i.e.,  $w_i = n_i / \sum_{i=1}^N n_i$ . Clearly, size  $n_i$  for all  $i = 1, 2, \dots, N$  should be large enough to represent the random process motions from individual seismic scenario. As a result, weighted ensemble population  $\{\Gamma\}$  with occurrence rate  $\bar{\lambda}$  is statistically equivalent to the aggregation of motion population  $\{\Gamma_i\}$  from individual scenario with rate  $\lambda_i$ . Then the ensemble population  $\{\Gamma\}$

can be characterized as a single random process and single stochastic FEM analysis is performed with PC-represented random process motions. Compared with PC-KL representation for each individual population  $\{\Gamma_i\}$ , the consequence of PC-KL expansion for ensemble population  $\{\Gamma\}$  is that larger dimension of PC is required since underlying random process of population  $\{\Gamma\}$  is more uncertain and less correlated among different times. If both individual population  $\{\Gamma_i\}$  and ensemble population  $\{\Gamma\}$  are accurately characterized by PC-KL expansion and propagated into uncertain structure through SFEM, EDP hazard can be calculated by either Equation (5) or Equation (6):

$$\lambda(EDP > z) = \sum_{i=1}^N \lambda_i(M_i, R_i, \Theta_i) P(EDP > z | \Gamma_i) \quad (5)$$

$$\lambda(EDP > z) = \bar{\lambda} P(EDP > z | \Gamma) \quad (6)$$

where  $P_i(EDP > z | \Gamma_i)$  is the failure probability conditioned on individual population  $\{\Gamma_i\}$  and  $P(EDP > z | \Gamma)$  is the failure probability conditioned on ensemble population  $\{\Gamma\}$ . Both Equation (5) and Equation (6) give consistent result for EDP hazard. The difference is that by using Equation (5), many more less expensive SFEM analyses are performed while using Equation (6) requires a single, yet more expensive SFEM analysis. When the number of scenarios  $N$  is small, it is practical to perform stochastic FEM analysis for each scenario and compute EDP hazard by Equation (5). The advantage is that controlling scenario can be identified through EDP hazard de-aggregation. However, when there are many seismic scenarios, quantifying ensemble population as a single random process through PC-KL expansion and performing single stochastic FEM analysis can be computationally more efficient.

## 2.1. Seismic source characterization

Seismic source characterization (SSC) and earthquake rupture forecast (ERF) are complex scientific issues. Earthquake occurrence rate tends to be comprehensively evaluated by multiple approaches, for example, using historical seismicity, geological information (e.g., long term slip rates and paleoseismic recurrence intervals) and geodetic information [30]. Assuming Poisson process of earthquake occurrence, annual occurrence rate  $\lambda^f$  of earthquakes on a fault can be estimated based on seismic moment balance [31]:

$$\lambda^f = \frac{\mu A \mathcal{S}}{\int_0^{M_{max}} E(M) f(M) dM} \quad (7)$$

where  $\mathcal{S}$  is annual slip rate,  $\mu$  is shear modulus of crust and  $A$  is fault area,  $f(M)$  is the probabilistic model of magnitude distribution, which

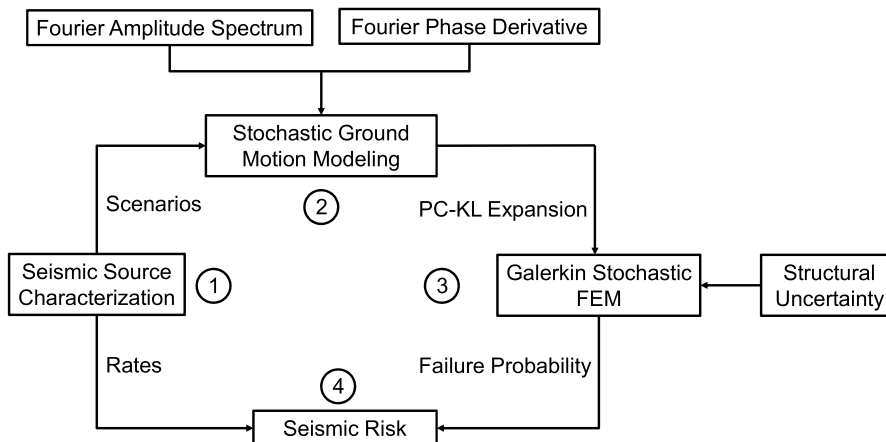


Fig. 1. Time domain intrusive framework for seismic risk analysis.

could be truncated exponential model, Young's and Coppersmith characteristic model [32], truncated Gaussian model, etc. The seismic moment of earthquake,  $E(M)$  with magnitude  $M$  is given as:

$$E(M) = 10^{1.5M+16.05} \quad (8)$$

In engineering practices, only earthquakes greater than certain magnitude  $M_{min}$  are considered, whose annual occurrence rate  $\bar{\lambda}^f$  is:

$$\bar{\lambda}^f = \lambda^f \int_{M_{min}}^{M_{max}} f(M) dM \quad (9)$$

Using probabilistic models of rupture area conditioned on magnitude  $f(A|M)$ , rupture width conditioned on rupture area  $f(W|A)$  [33], rupture location along strike (AS)  $f(Y)$  and down-dip (DD)  $f(Z)$ , distance metric  $R$  and other scenario metrics  $\Theta$ , for example, depth to the top of rupture plane  $Z_{top}$ , can be geometrically characterized as  $g(R, \Theta|M)$  for a given engineering site [34]. The discretized mutually exclusive scenarios  $\lambda_i(M_i, R_i, \Theta_i)$  in Equation (2) is then quantified as:

$$\lambda_i(M_i, R_i, \Theta_i) = \sum_{j=1}^m \bar{\lambda}_j^f \int_{\Lambda_i} f_j(M) g_j(R, \Theta|M) dM dR d\Theta \quad (10)$$

where  $m$  is the total number of active faults, subscript  $j$  denotes the probabilistic models and quantities specific to the  $j^{th}$  fault,  $\Lambda_i$  is the integral domain for the  $i^{th}$  discretized scenario with magnitude step  $\Delta M$ , distance step  $\Delta R$  and  $\Delta \Theta$  for any other scenario metrics  $\Theta$  if required:

$$\Lambda_i = \left[ M_i - \frac{\Delta M}{2}, M_i + \frac{\Delta M}{2} \right] \times \left[ R_i - \frac{\Delta R}{2}, R_i + \frac{\Delta R}{2} \right] \times \left[ \Theta_i - \frac{\Delta \Theta}{2}, \Theta_i + \frac{\Delta \Theta}{2} \right] \quad (11)$$

Many PSHA programs could perform SSC, e.g., HAZ45 [34]. It is noted that presented above are fundamental relations for seismic characterization of fault sources. For regions with unknown fault locations or having background seismicity, areal source should also be considered and characterized. See Refs. [35,36] for more details on seismic source characterization of areal source. Epistemic uncertainties in slip rate, magnitude distribution models and other parameters, which are typically considered with logic tree approach [37], are not considered here for simplicity. In addition, for some sites, authoritative estimates of magnitude, location and rate of earthquake ruptures could be determined from established regional earthquake rupture forecast (ERF) models, for example, UCERF3 [30] for California region.

## 2.2. Time domain stochastic ground motion modeling

Time domain uncertain motions can be simulated from stochastic FAS and Fourier phase derivative [11,38]. Specifically, uncertain FAS of seismic motions is modeled as Log-normal distributed random field [13,39] in frequency space, whose marginal median behavior is simulated by the stochastic method of Boore [11]. It is referred to as Boore03 approach hereafter. Boore03 approach simulates FAS using  $w^2$  radiated source spectrum [9] with modification for path and site effects, as shown in Equation (12):

$$FAS(f) = A_0(M_0, f) Z(R) \exp(-\pi f R / Q\beta) S(f) \exp(-\pi \kappa_0 f) \quad (12)$$

where  $M_0$  is the seismic moment;  $\beta$  is the source shear wave velocity;  $Z(R)$  and  $\exp(-\pi f R / Q\beta)$  represent the contribution from path effects;  $Z(R)$  is the geometrical spreading term as a function of distance  $R$ . Term  $\exp(-\pi f R / Q\beta)$  quantifies the anelastic attenuation as the inverse of the regional quality factor,  $Q$ . The site effects including site amplification through crustal velocity gradient and near surface attenuation are demonstrated by  $S(f)$  and  $\kappa_0$  filter  $\exp(-\pi \kappa_0 f)$ , respectively. Term  $A_0$  represents the radiated acceleration source spectrum, which could be characterized by single-corner-frequency model:

$$A_0(M_0, f) = CM_0 \left[ \frac{(2\pi f)^2}{1 + (f/f_0)^2} \right] \quad (13)$$

where  $f_0$  is the corner frequency, which in Brune's model [9] is related to source stress drop  $\Delta\sigma$  as follows:

$$f_0 = 4.9 \times 10^6 \beta (\Delta\sigma / M_0)^{1/3} \quad (14)$$

Boore03 approach is well-recognized for its simplicity and effectiveness to capture the marginal mean behavior of stochastic FAS. Bayless and Abrahamson [61] pointed out that the inter-frequency correlation structure of FAS random field is also important for seismic risk analysis. Misrepresenting-representing the correlation structure, e.g., assuming inter-frequency independence, would lead to underestimation of seismic risk. Therefore, inter-frequency correlation model for stochastic FAS developed recently [13,14] is adopted here.

Though the behavior of FAS was well studied, modeling Fourier phase angles is still challenging. Conventionally random phase info is simulated using stationary Gaussian white noise modulated by an envelope function. However, Montaldo et al. [40] stated that conventional Gaussian white noise approach could not reliably reproduce the non-stationarity of ground motions. For this reason, the use of phase difference  $\Delta\Phi$  was suggested by Ref. [41]. Using California strong ground motion data, Thráinsson and Kiremidjian [42] modeled phase differences as Beta distribution. However, the established phase difference models are affected by the signal length of each record. It is more stable to normalize phase difference by signal length and study the probabilistic model of phase derivative  $\dot{\Phi}$  defined as [38]:

$$\dot{\Phi} = \frac{\Delta\Phi}{\Delta f} \quad (15)$$

Based on 3551 ground motion records from PEER NGA-West 1 database, Baglio [15] found that the distribution of phase derivative is leptokurtic and fits well to Logistic model:

$$f(\dot{\Phi}; \mu, \sigma) = \frac{1}{4\sigma} \operatorname{sech}^2\left(\frac{\dot{\Phi} - \mu}{2\sigma}\right) \quad (16)$$

where  $\mu$  and  $\sigma$  are the mean and scale parameter of the Logistic distribution  $f(\dot{\Phi}; \mu, \sigma)$ ,  $\operatorname{sech}(\cdot)$  is the hyperbolic secant function. Following [15], the mean value  $\mu$  is a fixed parameter to position the distribution along the signal length. For example, setting mean parameter  $\mu$  equal to  $\pi/df$  would align the peak of uncertain seismic motions to the center of simulated signal length. The prediction equation of scale parameter  $\sigma$  is correlated to earthquake magnitude  $M$ , rupture distance  $R_{rup}$ ,  $V_{s30}$  and directivity index  $D_{Dir} = R_{typ} - R_{rup}$  with coefficients  $\alpha_1, \alpha_2, \beta_1 \sim \beta_4, \gamma_1$  and  $\gamma_2$  determined from maximum likelihood estimation:

$$\log(\sigma / \pi) = \alpha_1 + \alpha_2 \log[\beta_1 + 10^{\beta_2 M} + \beta_3 R_{rup} + \beta_4 \log(V_{s30})] + \gamma_1 + \gamma_2 D_{Dir} \quad (17)$$

Phase derivatives  $\dot{\Phi}(f)$  among frequency coordinates is modeled as Logistic distributed random field following exponential correlation with correlation length  $l_f = 0.05Hz$ :

$$\operatorname{Cov}(\dot{\Phi}(f_1), \dot{\Phi}(f_2)) = e^{-\frac{|f_1 - f_2|}{l_f}} \quad (18)$$

The methodology of time domain stochastic ground motion modeling is summarized below:

1. Compute marginal median of Log-normal distributed random field  $FAS(f)$  following Boore03 approach.
2. Generate realizations of Log-normal distributed random field  $FAS(f)$  according to the marginal estimation in step 1 and inter-frequency correlation model by Bayless and Abrahamson [14].

3. Determine the scale parameter  $\sigma$  of marginal Logistic model for phase derivative random field with Equation (17). Set mean value  $\mu$  to  $\pi/df$  for central peak [15].
4. Generate realizations of Logistic distributed random field  $\Phi(f)$  with marginal distribution from step 3 and exponential correlation structure.
5. Multiply realization of phase derivative in step 4 by frequency interval  $df$  to get realizations of phase difference  $\Delta\Phi(f)$ . Compute realizations of phase angles from  $\Delta\Phi(f)$ . First phase angle can be randomly set and would not affect the synthesis.
6. Inverse fourier transformation to time domain with realizations of FAS and FPS.

Time domain stochastic ground motion for a single scenario with magnitude  $M = 7$ , distance  $R_{rup} = 15\text{km}$  has been simulated following the above methodology. The detailed modeling parameters for source, path and site effects of this scenario are given in Table 1. The marginal median FAS is computed using program SMSIM developed by Ref. [44]. With reference to recent GMPE studies of FAS [39,45], marginal lognormal standard deviation of FAS has been adopted as total  $\sigma = 0.8 \ln$  units. The maximum modeling frequency  $f_{max}$  is 20Hz. It is noted that ergodic assumption was used in developing these GMPEs of FAS. A smaller value of marginal standard deviation can be used for non-ergodic probabilistic seismic risk analysis if additional source, path or site specific information is available.

Combining stochastic FAS with uncertain Fourier phase info, 500 realizations of time domain stochastic motions are synthesized. Fig. 2 shows three different synthesized accelerations. Large variability is observed, for example, peak ground acceleration could vary from  $1.8m/s^2$  to  $5.5m/s^2$ .

Spectral acceleration ( $S_a$ ) of 500 synthesized realizations are calculated and compared with weighted average prediction of five NGA West-2 GMPEs [2] with weights 0.22 for ASK14, 0.22 for BSSA14, 0.22 for CB14, 0.22 for CY14 and 0.12 for I14. From Fig. 3(a), median spectral acceleration  $S_a$  from simulated stochastic ground motion is in very good agreement with GMPE predictions for all period ordinates. No systematic bias is observed. Fig. 3(b) shows that the standard deviation of simulated response spectra is around 0.65  $\ln$  units, which is consistent with aleatory variability of  $S_a$  given by GMPEs. In other words, time domain stochastic ground motions simulated with aforementioned methodology could not only characterize the median behavior of  $S_a$  very well, but also carry desired amount of uncertainty that is consistent with empirical GMPEs.

**Table 1**

Source, path and site parameters for stochastic ground motion modeling of seismic scenario  $M = 7$ ,  $R_{rup} = 15\text{km}$ .

Parameter type	Name	Value
Source	Magnitude	$M = 7$
	Source density	$\rho_s = 2.8\text{g}/\text{cm}^3$
	Source velocity	$\beta = 3.6\text{km}/\text{s}$
	$w^2$ source spectrum	Single corner frequency with $\Delta\sigma = 8.0\text{MPa}$
	Fault type	Reverse fault $F_{rv} = 1$
Path	Dip angle	$45^\circ$
	Distance metrics	$R_{rup} = 15\text{km}$ , $R_{hyp} = 18\text{km}$ $R_{yb} = 12\text{km}$ , $R_x = -12\text{km}$
	Finite faults effects	Equivalent point source model [12] with $R_{ps} = 22.18\text{km}$
	Geometrical spreading	Hinged line segments model [43]
	Anelastic attenuation Q	Three line segments model by [11]
Site	Site amplification	$V_{s30} = 620\text{m}/\text{s}$ Table 4 of [12]
	$\kappa_0$ attenuation	$\kappa_0 = 0.03\text{s}$

The marginal distribution of simulated accelerations at all the time instances is observed to be Gaussian. Similar observation is also made by Ref. [24] from statistical analysis of seismic records. Therefore, time domain stochastic ground motions is modeled as a Gaussian distributed non-stationary random process. The random process would be represented with Hermite polynomial chaos as formulated in the next section.

It is worthwhile to mention that the random process incorporates much more information about uncertain ground motions than GMPE used in conventional PBEE. GMPE only quantifies the variability of selected IM, such as  $S_a$ , while the random process carries not only consistent variability of  $S_a$  but also any other important characteristics, e.g., PGA, CAV, etc. Realistic inter-frequency correlation of FAS [14] is captured. Non-stationarity of seismic motions is quantified through phase derivative modeling without using any modulation function. Compared with existing ground motion modeling techniques commonly adopted by reliability community, e.g., evolutionary power spectrum and white noise random phase spectrum, presented methodology is directly compatible with state-of-the-art seismic source characterization. It could explicitly account for specific source, path and site condition in both stochastic modeling of FAS and FPS. Many reliability analysis methods, such as probabilistic density evolution method [46] can be readily combined with the presented methodology and incorporated into the proposed risk analysis framework for PBEE.

### 2.3. Hermite polynomial chaos Karhunen-Loève expansion

This section formulates Hermite polynomial chaos Karhunen-Loève (PC-KL) expansion for general heterogeneous random field  $D(x, \theta)$  of arbitrary marginal distribution. Both uncertain motions and uncertain structure parameters can be represented with PC-KL expansion. To achieve this, we first represent heterogeneous random field  $D(x, \theta)$  of arbitrary marginal distribution through Hermite polynomial chaos of underlying Gaussian heterogeneous random field  $\gamma(x, \theta)$  up to order  $P$  [24,28]:

$$D(x, \theta) = \sum_{i=0}^P D_i(x) \Omega_i(\gamma(x, \theta)) \quad (19)$$

where  $\theta$  denotes the uncertainties. Functions  $\{\Omega_i\} = \{1, \gamma, \gamma^2 - 1, \gamma^3 - 3\gamma, \dots\}$  are orthogonal, zero mean ( $i \geq 1$ ) Hermite PC bases constructed from zero mean, unit variance kernel Gaussian random field  $\gamma(x, \theta)$ . Then at the second step, Gaussian random field  $\gamma(x, \theta)$  can be further decomposed by Karhunen-Loève (KL) theorem [29].

The deterministic PC coefficient field  $D_i(x)$  can be calculated through marginal distribution of  $D(x, \theta)$ , as shown in Equation (20), where  $\langle \cdot \rangle$  is the expectation operator.

$$D_i = \frac{\langle D \Omega_i \rangle}{\langle \Omega_i^2 \rangle} \quad (20)$$

The covariance structure of the original random field  $Cov_D(x_1, x_2)$  is mapped to the Gaussian covariance kernel  $Cov_\gamma(x_1, x_2)$  as:

$$Cov_D(x_1, x_2) = \sum_{i=1}^P D_i(x_1) D_i(x_2) i! Cov_\gamma(x_1, x_2) \quad (21)$$

The Gaussian covariance kernel  $Cov_\gamma(x_1, x_2)$  can be eigen-decomposed into probabilistic spaces up to dimension  $M$ , according to Karhunen-Loève (KL) theorem [29]:

$$\gamma(x, \theta) = \sum_{i=1}^M \sqrt{\lambda_i} f_i(x) \xi_i(\theta) \quad (22)$$

where  $\{\xi_i(\theta)\}$  are the multidimensional, orthogonal, zero mean and unit variance Gaussian random variables, and  $\lambda_i$  and  $f_i(x)$  are the eigenvalues and eigen-vectors of the covariance kernel  $Cov_\gamma(x_1, x_2)$  that

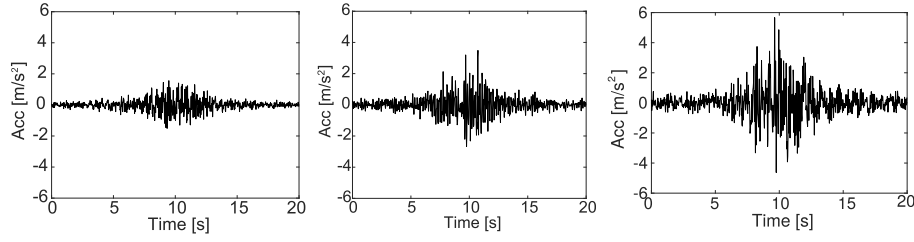


Fig. 2. Realizations of uncertain acceleration time series population.

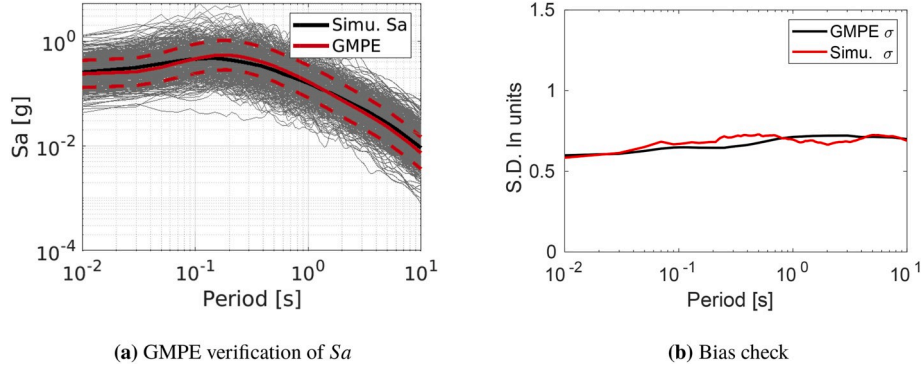


Fig. 3. Verification of simulated stochastic motions: (a) Check median spectral acceleration  $S_a$  with NGA West-2 GMPE (b) Check aleatory variability of simulation spectral acceleration  $S_a$ .

satisfy Fredholm's integral equation of the second kind [28].

Combining Equations (19) and (22), the resultant PC-KL representation of general random field  $D(x, \theta)$  is obtained as,

$$D(x, \theta) = \sum_{i=0}^K d_i(x) \Psi_i(\{\xi_j(\theta)\}) \quad (23)$$

where  $\{\Psi_i\}$  are multi-dimensional orthogonal Hermite PC bases of order  $P$  constructed from  $M$  dimensional probabilistic space (i.e.,  $\{\xi_j(\theta)\}$ ,  $j = 1, 2, \dots, M$ ). The total number of multidimensional Hermite PC bases  $K$  is related to order  $P$  and dimension  $M$  as  $K = 1 + \sum_{s=1}^P \frac{1}{s!} \prod_{j=0}^{s-1} (M + j)$ .

By equating two representations of  $D(x, \theta)$  in Equations (19) and (23), the coefficients of multi-dimensional Hermite PC are derived as:

$$d_i(x) = \frac{p!}{\langle \Psi_i \rangle^2} D_p(x) \prod_{j=1}^p \frac{\sqrt{\lambda_{k(j)}} f_{k(j)}(x)}{\sqrt{\sum_{m=1}^M (\sqrt{\lambda_m} f_m(x))^2}} \quad (24)$$

where  $p$  is the order of the polynomial  $\Psi_i$ . From Equation (23), PC synthesized marginal mean and variance of the original heterogeneous random field can be calculated as:

$$\langle D(x, \theta) \rangle = d_0(x) \quad (25)$$

$$\text{Var}(D(x, \theta)) = \sum_{i=1}^K d_i^2(x) \langle \Psi_i^2 \rangle \quad (26)$$

PC-synthesized correlation structure can also be computed as:

$$\text{Cov}_D(x_1, x_2) = \frac{\sum_{i=1}^K d_i(x_1) d_i(x_2) \langle \Psi_i^2 \rangle}{\sqrt{\text{Var}(D(x_1)) \text{Var}(D(x_2))}} \quad (27)$$

Equations (25)–(27) can be used to compare the PC-synthesized statistics with statistics of original random field  $D(x, \theta)$  and check the goodness of PC-KL expansion.

#### 2.4. Galerkin stochastic finite element method

Stochastic Galerkin approach intrusively solves the stochastic partial differential equations (PDE) with optimal convergence [22,24]. Compared to deterministic finite element method (FEM), Galerkin stochastic FEM introduces spectral discretization of probabilistic domain in addition to the spatial and temporal discretization. Using standard spatial FEM discretization, unknown displacement random field  $u(x, t, \theta)$  can be expressed with shape function  $N_i(x)$  and uncertain displacement  $u_i(t, \theta)$  at nodes:

$$u(x, t, \theta) = \sum_{i=1}^N N_i(x) u_i(t, \theta) \quad (28)$$

Uncertain displacement at nodes  $u_i(t, \theta)$ , can be further represented with aforementioned multidimensional Hermite PC basis  $\varphi_j(\{\xi_r(\theta)\})$  of dimension  $M^u$ , order  $P^u$ :

$$u_i(t, \theta) = \sum_{j=0}^{K^u} u_{ij}(t) \varphi_j(\{\xi_r(\theta)\}) \quad (29)$$

Combining Equations (28) and (29), spatial-probabilistic discretized expression of  $u(x, t, \theta)$  is given:

$$u(x, t, \theta) = \sum_{i=1}^N \sum_{j=0}^{K^u} N_i(x) u_{ij}(t) \varphi_j(\{\xi_r(\theta)\}) \quad (30)$$

Galerkin weak formulation of stochastic partial differential equations of motion can then be written in the following form:

$$\sum_e \left[ \int_{D_e} N_m(x) \rho(x) N_n(x) dV \ddot{u}_n(t, \theta) + \int_{D_e} B_m(x) E(x, \theta) B_n(x) dV u_n(t, \theta) - f_m(t, \theta) \right] = 0 \quad (31)$$

where  $\sum_e$  denotes the assembly procedure over all finite elements, while

$\rho(\mathbf{x})$  is deterministic material density field. The shape function gradient function  $B_n(\mathbf{x})$  is given as:

$$B_n(\mathbf{x}) = \nabla N_n(\mathbf{x}) \quad (32)$$

In Equation (31),  $E(\mathbf{x}, \theta)$  is uncertain tangential stiffness matrix, while  $f_m(t, \theta)$  is uncertain global force vector that incorporates various elemental contributions.

Expansion of uncertain stiffness matrix  $E(\mathbf{x}, \theta)$ , and uncertain force vector  $f_m(t, \theta)$  into Hermite PC bases  $\Psi_k(\{\xi_r(\theta)\})$  and  $\psi_l(\{\xi_r(\theta)\})$  of dimension  $M^E$ , order  $P^E$  and dimension  $M^f$ , order  $P^f$ , respectively, yields:

$$E(\mathbf{x}, \theta) = \sum_{k=0}^{K^E} E_k(\mathbf{x}) \Psi_k(\{\xi_r(\theta)\}) \quad (33)$$

$$f_m(t, \theta) = \sum_{l=0}^{K^f} f_{ml}(t) \psi_l(\{\xi_r(\theta)\}) \quad (34)$$

By combining equations (29), (33) and (34) and equation (31), one obtains:

$$\begin{aligned} & \sum_e \left[ \int_{D_e} N_m(\mathbf{x}) \rho(\mathbf{x}) N_n(\mathbf{x}) dV \sum_{j=0}^{K^u} \ddot{u}_{nj} \varphi_j(\{\xi_r(\theta)\}) - \sum_{l=0}^{K^f} f_{ml} \psi_l(\{\xi_r(\theta)\}) \right. \\ & \left. + \int_{D_e} B_m(\mathbf{x}) \sum_{k=0}^{K^E} E_k(\mathbf{x}) \Psi_k(\{\xi_r(\theta)\}) B_n(\mathbf{x}) dV \sum_{j=0}^{K^u} u_{nj} \varphi_j(\{\xi_r(\theta)\}) \right] = 0 \end{aligned} \quad (35)$$

By performing Galerkin projection of Equation (35) onto PC bases  $\varphi_i(\{\xi_r(\theta)\})$ , to minimize the residual, system of deterministic ordinary differential equations (ODE) involving temporal derivative of unknown PC coefficients  $u_{nj}$ , is developed:

$$M_{minj} \ddot{u}_{nj} + K_{minj} u_{nj} = F_{mi} \quad (36)$$

where mass tensor/matrix  $M_{minj}$  is given by equation (37):

$$M_{minj} = \sum_e \int_{D_e} N_m(\mathbf{x}) \rho(\mathbf{x}) N_n(\mathbf{x}) dV \langle \varphi_i \varphi_j \rangle \quad (37)$$

stochastic stiffness tensor/matrix  $K_{minj}$  is given by equation (38):

$$K_{minj} = \sum_{k=0}^{K^E} \sum_e \int_{D_e} B_m(\mathbf{x}) E_k(\mathbf{x}) B_n(\mathbf{x}) dV \langle \Psi_k \varphi_i \varphi_j \rangle \quad (38)$$

and stochastic force tensor/vector  $F_{mi}$  is given by equation (39)

$$F_{mi} = \sum_{l=0}^{K^f} f_{ml} \langle \psi_l \varphi_i \rangle \quad (39)$$

In Equations (37)–(39), terms  $\langle \varphi_i \varphi_j \rangle$ ,  $\langle \psi_l \varphi_i \rangle$  and  $\langle \Psi_k \varphi_i \varphi_j \rangle$  are the ensemble average tensors of double-product and tri-product of different PC bases. These ensemble average tensors could be pre-computed and used to construct the stochastic mass matrix  $M_{minj}$  and stochastic stiffness matrix  $K_{minj}$ . It is noted that Einstein's notation for tensor indices summation is assumed throughout [47].

The deterministic system of ordinary differential equations (ODE) from Equation (36), can be integrated in time using dynamic integrator algorithms, for example Newmark method [48], or Hilber-Hughes-Taylor  $\alpha$ -method [49]. Result of such time marching solution will be time histories of displacement PC coefficients  $u_{nj}$ . Those

time evolving displacement PC coefficients  $u_{nj}$  can then be used to develop complete probabilistic dynamic finite element response. With resulting complete probabilistic dynamic finite element response, any damage measure, in fact all damage measures related to EDP(s) can be applied to trace the failure probability  $P_i(EDP > z | \Gamma_i)$  or  $P(EDP > z | \Gamma)$ . EDP hazard can then be computed according to Equations (5) and (6).

The above formulation of Galerkin stochastic FEM is complete for linear elastic problem with constant uncertain elastic stiffness matrix  $E(\mathbf{x}, \theta)$ . For nonlinear, inelastic problems, additional formulation of stochastic elastic-plastic FEM (SEPFEM) is required and relies on recent developments [20–23,50–52]. One of the challenges of the SEPFEM lies in the development of the probabilistic elastic-plastic stiffness at the constitutive level that is to be used for finite element level computations. Eulerian-Lagrangian form of the Fokker-Planck-Kolmogorov (FPK) equation has been successfully used to obtain probabilistic stress solutions [20–22]. It is noted in order to produce uncertain stiffness, least square optimization and linearization techniques [22,23] are used.

To this end, in one dimension (1D), elastic plastic material model with vanishing elastic region is used in conjunction with Armstrong-

Fredrick nonlinear kinematic hardening [53,54]. This approach simplifies modeling, as elastic plastic response directly follows Armstrong-Fredrick nonlinear equation. For the approach proposed here, probabilistic nonlinear response between inter-story restoring force  $F^R$  and inter-story drift  $\eta$  is formulated through direct PC-based Galerkin intrusive probabilistic modeling of Armstrong-Fredrick hysteretic behavior.

In incremental form, Armstrong-Fredrick kinematic hardening relation [53] between inter-story restoring force  $F^R$  and inter-story drift  $\eta$  can be written as:

$$dF^R = H_a d\eta - C_r F^R |d\eta| \quad (40)$$

where  $H_a$  and  $C_r$  are model parameters. By setting  $dF^R = 0$ , the ultimate inter-story restoring force becomes  $F_{max}^R = H_a/C_r$ . The tangential stiffness  $E(F^R)$  is a function of restoring force  $F^R$ :

$$E(F^R) = \frac{dF^R}{d\eta} = H_a - C_r F^R \operatorname{sgn}(d\eta) \quad (41)$$

where  $\operatorname{sgn}(\cdot)$  is the sign function. Equation (41) can be written as:

$$E(F^R) = H_a \pm C_r F^R \quad (42)$$

where + sign is taken for negative inter-story drift  $d\eta$  and – sign is taken for positive inter-story drift  $d\eta$ . In the general probabilistic setting, model parameters  $H_a$  and  $C_r$  can be uncertain and modeled as random fields  $H_a(\mathbf{x}, \theta)$  and  $C_r(\mathbf{x}, \theta)$ . By applying PC expansion with Hermite PC bases  $\phi_i(\{\xi_r(\theta)\})$  to those two model parameters, the following equations are obtained:

$$H_a(\mathbf{x}, \theta) = \sum_{i=0}^P H_{ai}(\mathbf{x}) \phi_i(\{\xi_r(\theta)\}) \quad (43)$$

$$C_r(\mathbf{x}, \theta) = \sum_{i=0}^P C_{ri}(\mathbf{x}) \phi_i(\{\xi_r(\theta)\}) \quad (44)$$

The inter-story drift increments  $d\eta(\mathbf{x}, \theta)$ , that represent input to the constitutive driver (Equation (40)) are also uncertain due to the probabilistic structural response  $u(\mathbf{x}, t, \theta)$ :

$$d\eta(\mathbf{x}, \theta) = \sum_{i=0}^P d\eta_i(\mathbf{x}) \phi_i(\{\xi_r(\theta)\}) \quad (45)$$

As a result, probabilistic incremental restoring force  $dF^R(\mathbf{x}, \theta)$  and probabilistic tangential stiffness  $E(\mathbf{x}, \theta)$  are then:

$$dF^R(\mathbf{x}, \theta) = \sum_{i=0}^P dF_i^R(\mathbf{x}) \phi_i(\{\xi_r(\theta)\}) \quad (46)$$

$$E(\mathbf{x}, \theta) = \sum_{i=0}^P E_i(\mathbf{x}) \phi_i(\{\xi_r(\theta)\}) \quad (47)$$

Substituting Equation (43) ~ 47 into Equations (40) and (42) and applying Galerkin projection on PC basis  $\phi_i\{\xi_r(\theta)\}$  yields:

$$\sum_{m=0}^P dF_m^R \langle \phi_m \phi_i \rangle = \sum_{j=0}^P \sum_{k=0}^P H_{aj} d\eta_k \langle \phi_j \phi_k \phi_i \rangle \pm \sum_{l=0}^P \sum_{n=0}^P \sum_{s=0}^P C_{rl} F_n^R d\eta_s \langle \phi_l \phi_n \phi_s \phi_i \rangle \quad (48)$$

$$\sum_{i=0}^P E_m \langle \phi_m \phi_i \rangle = \sum_{j=0}^P H_{aj} \langle \phi_j \phi_i \rangle \pm \sum_{l=0}^P \sum_{n=0}^P C_{rl} F_n^R \langle \phi_l \phi_n \phi_i \rangle \quad (49)$$

By using the orthogonality of Hermite PC bases  $\langle \phi_i \phi_j \rangle = 0$  for  $i \neq j$ , solutions to the unknown PC coefficients of incremental inter-story force  $dF^R(\mathbf{x}, \theta)$  and inter-story stiffness  $E(\mathbf{x}, \theta)$  can be written as:

$$dF_i^R = \frac{1}{\text{Var}[\phi_i]} [H_{aj} d\eta_k \langle \phi_j \phi_k \phi_i \rangle \pm C_{rl} F_n^R d\eta_s \langle \phi_l \phi_n \phi_s \phi_i \rangle] \quad (50)$$

$$E_i = H_{ai} \pm \frac{1}{\text{Var}[\phi_i]} C_{rl} F_n^R \langle \phi_l \phi_n \phi_i \rangle \quad (51)$$

where  $\langle \cdot \rangle$  is the expectation operator.  $\text{Var}[\phi_i]$  is the scalar variance of PC basis  $\phi_i\{\xi_r(\theta)\}$ , which equals to  $\langle \phi_i^2 \rangle$ . It is noted that in the above equations, Einstein's tensor summation notation is used with index  $i$  as a free index. Terms  $\langle \phi_j \phi_k \phi_i \rangle$ ,  $\langle \phi_l \phi_n \phi_i \rangle$  and  $\langle \phi_l \phi_n \phi_s \phi_i \rangle$  are the expectation of triple and quadruple product of PC basis  $\phi_i\{\xi_r(\theta)\}$ .

The above 1D formulation for SEPFEM is implemented in the context of explicit, forward Euler algorithm. The expanded stiffness matrix  $K_{minj}$  is constructed using stiffness PC coefficients  $^{(n)}E_i$  at step  $n$  following

Equation (38). Displacement PC coefficients  $^{(n+1)}u_{nj}$  of step  $n+1$  are then solved by applying force vector  $^{(n+1)}F_{mi}$  and using stiffness matrix  $K_{minj}$  within Equation (36). Following that, incremental inter-story drift PC coefficients  $^{(n+1)}d\eta_i$  are calculated from displacement response  $^{(n+1)}u_{nj}$  and incremental uncertain restoring force  $^{(n+1)}dF_i^R$  can be quantified as:

$$^{(n+1)}dF_i^R = \frac{1}{\text{Var}[\phi_i]} [H_{aj} ^{(n+1)}d\eta_k \langle \phi_j \phi_k \phi_i \rangle \pm C_{rl} ^{(n)}F_n^R d\eta_s \langle \phi_l \phi_n \phi_s \phi_i \rangle] \quad (52)$$

Updating the restoring force  $^{(n+1)}F_i^R$  is then:

$$^{(n+1)}F_i^R = ^{(n)}F_i^R + ^{(n+1)}dF_i^R \quad (53)$$

while new stiffness PC coefficients  $^{(n+1)}E_i$  at step  $n+1$  are then:

$$^{(n+1)}E_i = H_{ai} \pm \frac{1}{\text{Var}[\phi_i]} C_{rl} ^{(n+1)}F_n^R \langle \phi_l \phi_n \phi_i \rangle \quad (54)$$

### 3. Illustrative example

To illustrate the proposed framework, seismic risk of a typical eight story shear frame structure that has been studied by many researchers [46,55–57], is developed. The frame structure is shown in Fig. 4.

The hysteretic restoring force versus inter-story drift behavior is described by Armstrong-Fredrick model presented in section 2.4. Material parameter  $H_a$  of Armstrong-Fredrick model is assumed to be Gaussian distributed random field with 15% coefficient of variation. Means of material parameter  $H_a$  are given for different floors as:  $H_{a1} \sim H_{a2} 1.59 \times 10^7 \text{N/m}$ ,  $H_{a3} \sim H_{a6} 1.66 \times 10^7 \text{N/m}$  and  $H_{a7} \sim H_{a8} 1.76 \times 10^7 \text{N/m}$ . The correlation structure of parameter  $H_a$  is assumed to be exponential between different floors, with correlation length of  $l_c = 10$  floors. Material parameter  $C_r$  is assumed to be  $C_r = 17.6 \text{ 1/m}$ . The resultant mean hysteretic behavior of first floor is also shown in Fig. 4. Floor masses are assumed to be deterministic. Rayleigh damping  $C = \alpha M + \beta K$  is used with parameters  $\alpha$  and  $\beta$  chosen to be  $\alpha = 0.22 \text{ Hz}$  and  $\beta = 0.008\text{s}$ . Other structure modeling parameters are given in Table 2. Those parameters are determined from Ref. [46]. Parameters  $H_a$  and  $C_r$  are calibrated to match the hysteretic behavior shown in Ref. [46].

**Table 2**  
Parameters of the eight-story shear frame structure.

$h_0$ [m]	$h$ [m]	$m_1 \sim m_2$ [kg]	$m_3 \sim m_4$ [kg]	$m_5 \sim m_6$ [kg]	$m_7 \sim m_8$ [kg]
4	3	$2 \times 10^5$	$2.2 \times 10^5$	$2.4 \times 10^5$	$2.5 \times 10^5$

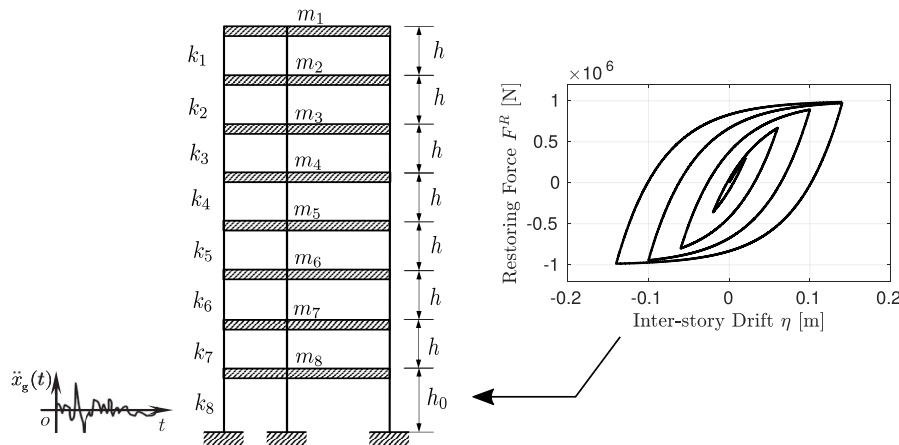


**Fig. 4.** Eight-story shear frame structure with uncertain floor stiffness under non-stationary seismic motions.



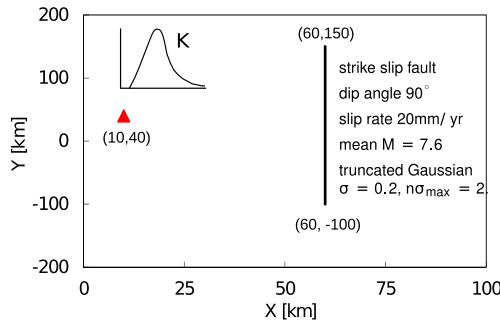


Fig. 5. Seismic risk analysis of an eight-story shear frame structure (red triangle) with uncertain stiffness  $K$  subjected to earthquakes from a strike slip fault (black line). (For interpretation of the references to colour in this figure legend, the reader is referred to the Web version of this article.)

**Table 3**  
Parameters for seismic source characterization (SSC) of the strike slip fault.

Parameter	Value
Fault length	250km
Fault width	15km
Dip angle	90°
Slip rate $\mathcal{S}$	20mm/yr
Style of faulting	Strike slip
$f(M)$	Truncated normal with $\sigma = 0.2 n\sigma_{max} = 2$ [34]
$f(A M)$	Delta function at $\log(A) = M - 4$
$f(W A)$	Delta function at $W = \sqrt{1.5A}$ , limited to fault width
$f(Y)$	Uniform distribution
$f(Z)$	Uniform distribution

**Table 4**  
Seismic scenarios for the strike slip fault.

Scenario ID	$M$	$R_{rup}$ [km]	Annual rate $\lambda(M, R_{rup})$
1	7.3	56	$9.54 \times 10^{-4}$
2	7.5	56	$2.40 \times 10^{-3}$
3	7.7	56	$2.40 \times 10^{-3}$
4	7.9	56	$9.54 \times 10^{-4}$

### 3.1. Seismic source characterization

The structure is located at coordinate (10km, 40km), 50km away from a strike slip fault with 90° dip angle, as shown in Fig. 5.

The fault length is 250km with annual slip rate of 20mm/yr. Detailed

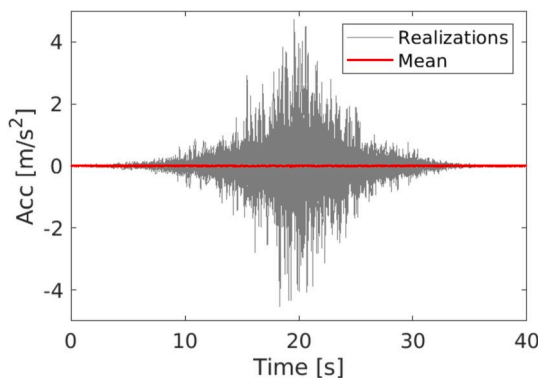


Fig. 6. Realizations of uncertain seismic motions for scenario  $M = 7.3, R_{rup} = 56km$ .

geometry and model parameters for SSC of the strike slip fault are given in Table 3.

Mean characteristic magnitude of the fault  $\bar{M}$  is 7.6, and is related to fault area  $A$  [33] as.

$$\bar{M} = \log(A) + 4 \quad (55)$$

Only earthquakes with magnitude greater than 5 (i.e.  $M_{min} = 5$ ) are considered. Following the procedure of SSC in section 2.1, annual rate of earthquakes occurring on the fault is  $\bar{\lambda} = 0.0067/\text{yr}$ . Probabilistic scenario space  $\lambda(M, R, \theta)$  is discretized into four mutually exclusive scenario events  $S_i(M_i, R_i, \Theta_i)$  as shown in Table 4. The computation is performed with probabilistic seismic hazard analysis program HAZ45 [34] using 0.2 for magnitude step  $\Delta M$  and 2km for distance step  $\Delta R$ .

### 3.2. Time domain stochastic ground motion modeling and representation

For each characterized seismic scenario  $S_i(M_i, R_i, \Theta_i)$ , 500 realizations  $\{\Gamma_i\}$  of time domain uncertain motions are simulated using methodology described in section 2.2. Fig. 6 shows the first 200 realizations of simulated motions for earthquake scenario 1 with  $M = 7.3, R_{rup} = 56km$ .

In this study, ground motion populations from four different scenarios are combined into a single population  $\Gamma$  using Equation (3) and modeled as a non-stationary random process. The random process is represented by multi-dimensional Hermite polynomial chaos (PC) following the technique formulated in section 2.3. Since marginal distribution of the random process is observed to be Gaussian (section 2.2), theoretically, PC representation with order 1 is sufficient. The dimension of PC basis needs to be carefully chosen to reconstruct the correlation structure of the original random process. To ensure the accuracy of PC-KL representation, following error measurements are defined and evaluated:

- The absolute error on marginal mean of the random process:

$$\epsilon_m = \frac{1}{N_t} \sum_{k=1}^{N_t} |\mu(t_k) - \hat{\mu}(t_k)| \quad (56)$$

- The absolute error on marginal standard deviation of the random process:

$$\epsilon_{std} = \frac{1}{N_t} \sum_{k=1}^{N_t} |\sigma(t_k) - \hat{\sigma}(t_k)| \quad (57)$$

**Table 5**  
Error in probabilistic characterization of non-stationary acceleration and displacement random process using PC-KL expansion with different dimensions.

Dimension of PC	Dim. 20	Dim. 70	Dim. 150	Dim. 300
Displacement mean error $\epsilon_m$	$8.63 \times 10^{-9}$	$8.63 \times 10^{-9}$	$8.63 \times 10^{-9}$	$8.63 \times 10^{-9}$
Displacement S.D. error $\epsilon_{std}$	$1.28 \times 10^{-7}$	$1.28 \times 10^{-7}$	$1.28 \times 10^{-7}$	$1.28 \times 10^{-7}$
Displacement correlation error $\epsilon_{corr}$	0.059	$2.26 \times 10^{-4}$	$8.27 \times 10^{-6}$	$3.06 \times 10^{-7}$
Acceleration mean error $\epsilon_m$	$9.84 \times 10^{-9}$	$9.84 \times 10^{-9}$	$9.84 \times 10^{-9}$	$9.84 \times 10^{-9}$
Acceleration S.D. error $\epsilon_{std}$	$1.23 \times 10^{-7}$	$1.23 \times 10^{-7}$	$1.23 \times 10^{-7}$	$1.23 \times 10^{-7}$
Acceleration correlation error $\epsilon_{corr}$	0.185	0.091	0.053	0.028

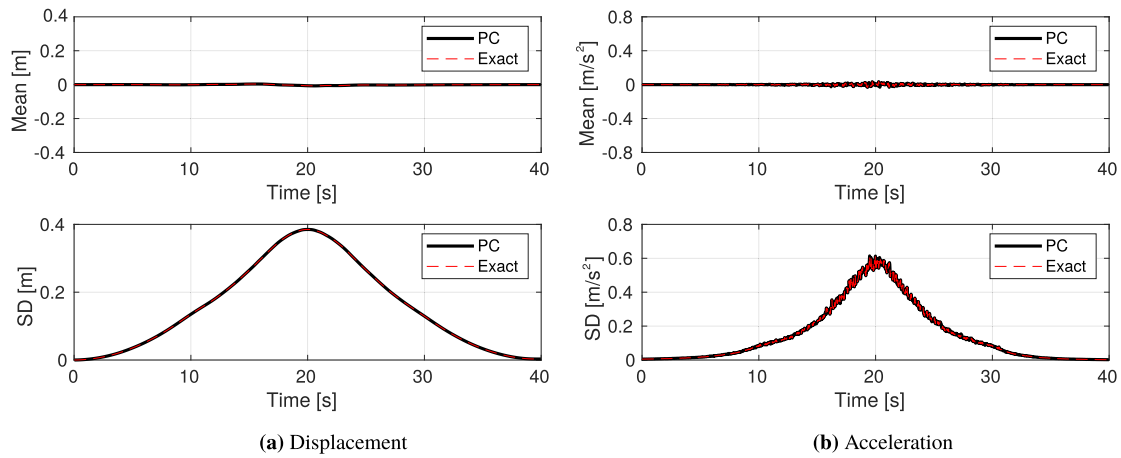


Fig. 7. Comparison between PC-synthesized (black line) marginal mean and marginal standard deviation (SD) and statistics of simulated ground motion realizations (red line). (For interpretation of the references to colour in this figure legend, the reader is referred to the Web version of this article.)

- The absolute error on correlation of the random process:

$$\epsilon_{corr} = \frac{1}{N_t^2} \sum_{k=1}^{N_t} \sum_{l=1}^{N_t} |Cov(t_k, t_l) - \widehat{Cov}(t_k, t_l)| \quad (58)$$

where  $\mu(t_k)$ ,  $\sigma(t_k)$  and  $Cov(t_k, t_l)$  are the marginal mean, marginal standard deviation and correlation field of simulated ground motion population  $\Gamma$ . Terms  $\widehat{\mu}(t_k)$ ,  $\widehat{\sigma}(t_k)$  and  $\widehat{Cov}(t_k, t_l)$  are statistics calculated from PC representation of the random process from Equations (25)–(27). Term  $t_k$  denotes the  $k^{th}$  time instance and  $N_t$  is the total number of time instances.

Hermite PC bases of order 1, dimension 20, 70, 150 and 300 are examined for PC-KL expansion of random process motions. The errors for different PC bases are given in Table 5.

It can be observed that in all the four cases marginal behavior of the random process motions is well captured with very small magnitudes of errors  $\epsilon_m$  and  $\epsilon_{std}$ . As shown in Fig. 7, synthesized marginal mean and marginal standard deviation from PC representation match very well with statistics of simulated motions.

As the dimension of PC increases, the relative error of correlation structure decreases while the computational cost in stochastic FEM increases. It is noted that PC dimension 70 is already adequate to capture the relatively smooth random displacement correlation field. However, acceleration correlation field synthesized from PC dimension 70 is overestimated among many time steps. PC dimension 150 and 300 approximate acceleration correlation structure much better. Eventually, considering both accuracy and efficiency, Hermite PC of order 1, dimension 150 is used to spectrally discretize the random process

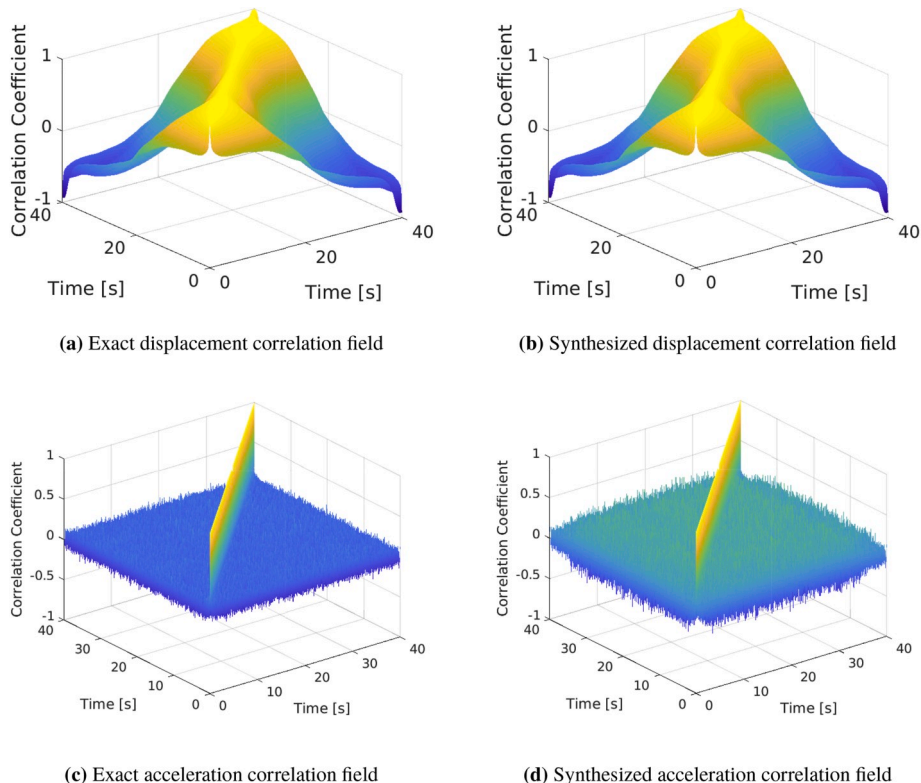


Fig. 8. Verification of PC synthesized acceleration and displacement correlation field with PC dimension 150.

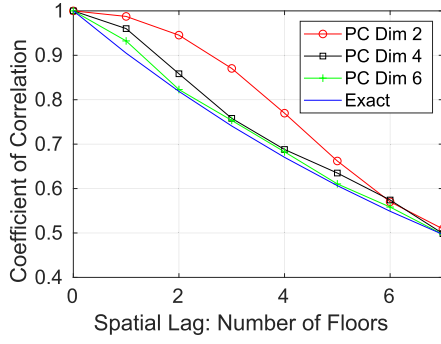


Fig. 9. Characterization of exponential correlation (correlation length  $l_c = 10$  floors) of uncertain structural parameter  $H_a(x, \theta)$  using PCs of different dimensions.

seismic motions in stochastic FEM analysis. The comparison between the exact correlation structure and the PC synthesized correlation structure is shown in Fig. 8.

### 3.3. Stochastic Galerkin FEM analysis and seismic risk

In order to perform stochastic Galerkin FEM analysis, it is also necessary to characterize the randomness of stiffness of the structural system. In order to do that, Hermite PCs of dimension 2, 4 and 6 is used for capturing the exponential correlation structure of random field parameter  $H_a(x, \theta)$ . It can be observed from Fig. 9 that PC dimension 4

can reasonably well reconstruct the correlation of  $H_a(x, \theta)$ .

With PC characterized structural parameters, the probabilistic hysteretic behavior of restoring force versus inter-story drift can be intrusively modeled following the stochastic Galerkin technique formulated in section 2.4. Fig. 10 shows the probabilistic response of restoring force of the first floor under cyclic loading.

Verification of developed constitutive modeling is performed using 10,000 Monte Carlo simulations and shown in Fig. 10 as well. It can be seen that PC-based intrusive probabilistic hysteresis modeling produces almost the same response as Monte Carlo simulations. It is noted that intrusive probabilistic approach is approximately 2000 times faster than corresponding Monte Carlo modeling.

With both uncertain seismic motions (dimension 150) and uncertain structural parameters (dimension 4) represented by Hermite PCs, probabilistic structural displacement is described in 154 dimensional probabilistic space of Hermite PCs. The unknown time varying PC coefficients, that contain all the information about the probabilistic evolution of structural response, are intrusively solved using developed Galerkin SEPFEM (section 2.4). With these solved PC coefficients, a polynomial chaos based surrogate model is analytically established [58]. After that, any probabilistic structural dynamic response can be easily reconstructed. Time evolving mean, standard deviation (SD) and correlation field of any resulting field of interest can be directly evaluated through Equations (25)–(27). By efficiently sampling the PC surrogate model, marginal or joint PDF of any structural response of interest can also be obtained through kernel density estimation.

For example, Fig. 11 shows the time evolving mean and standard deviation (SD) of the first and top floor deformation relative to the ground.

Due to inelastic, elastic-plastic response, uncertain permanent

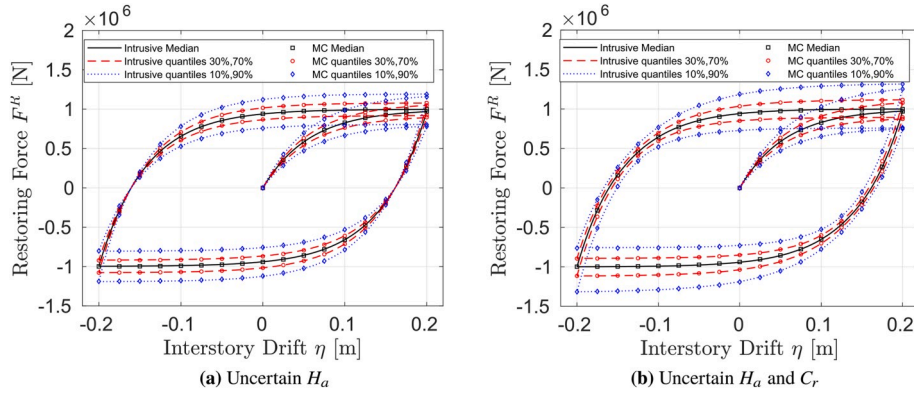


Fig. 10. Intrusive probabilistic modeling of Armstrong-Frederick hysteretic behavior and verification with Monte Carlo simulation: (a) Gaussian distributed  $H_a$  with mean  $1.76 \times 10^7$  N/m and 15% coefficient of variation (COV),  $C_r = 17.6$ . (b) Gaussian distributed  $H_a$  with mean  $1.76 \times 10^7$  N/m and 15% coefficient of variation (COV), Gaussian distributed  $C_r$  with mean 17.6 and 15% COV.

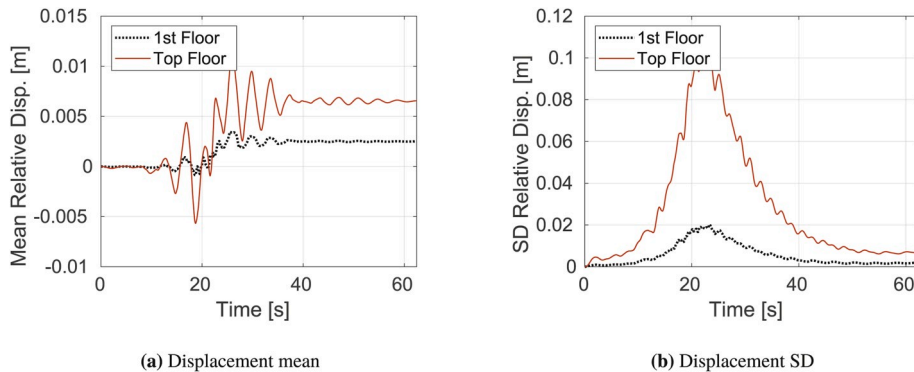


Fig. 11. Time evolving mean and standard deviation (SD) of the first and top floor deformation relative to the ground.

deformation is observed in both mean and standard deviation of floor deformation. It is noted that the deformation of top floor presents much larger variability than that of the first floor.

Two typical engineering demand parameters (EDPs) are selected for seismic risk analysis: Maximum inter-story drift ratio (MIDR) and Peak floor acceleration (PFA) [59,60]. We define MIDR as a function of probabilistic dynamic floor displacement:

$$MIDR_i(\theta) = \max_{t \in [0, T]} \left\{ \frac{|u_i(t, \theta) - u_{i-1}(t, \theta)|}{H_i} \right\} \quad (59)$$

$$MIDR(\theta) = \max_{i \in [1, 8]} \max_{t \in [0, T]} \left\{ \frac{|u_i(t, \theta) - u_{i-1}(t, \theta)|}{H_i} \right\} \quad (60)$$

where  $MIDR_i(\theta)$  and  $u_i(t, \theta)$  are the probabilistic MIDR and displacement of the  $i^{th}$  floor, respectively, and  $H_i$  is the floor height, while probabilistic MIDR of the whole shear frame structure is given as  $MIDR(\theta)$ .

Probabilistic floor accelerations are defined as:

$$PFA_i(\theta) = \max_{t \in [0, T]} \{ |\ddot{u}_i(t, \theta)| \} \quad (61)$$

$$PFA(\theta) = \max_{i \in [1, 8]} \max_{t \in [0, T]} \{ |\ddot{u}_i(t, \theta)| \} \quad (62)$$

where  $PFA_i(\theta)$  and  $\ddot{u}_i(t, \theta)$  are the probabilistic PFA and acceleration of the  $i^{th}$  floor, respectively, while  $PFA(\theta)$  is the probabilistic PFA of the whole structure. Since both probabilistic displacements  $u_i(t, \theta)$  and probabilistic accelerations  $\ddot{u}_i(t, \theta)$  are well defined through resulting PC coefficients, probabilistic response of MIDR and PFA are readily available through Equations (59)–(62).

For example problem, the probability density evolution of  $MIDR(\theta)$  is shown in Fig. 12.

At  $t = 0s$ , the structure is deterministically at rest, therefore, the PDF of  $MIDR$  tends to infinity, i.e., a delta function centered at zero and as such is not shown in Fig. 12. Fig. 13 shows typical PDFs at three different times.

It can be observed that PDF of MIDR is dispersing during first half of the seismic loading, while toward the end of the loading, it shows high kurtosis, due to reduced variation in input excitations.

The PDFs of MIDR of several different floors (1st, 3rd, 6th and top floor) and the whole frame structure are shown in Fig. 14(a). It is observed that the mean of MIDR increases along with larger dispersion, from the top to the bottom floor. This is expected considering the increase of shear force from the top floor to the base. The MIDR PDF of the first floor almost overlaps with that of the whole structure, which indicates that the maximum inter-story drift happens at first floor. From the probabilistic distribution of MIDR, exceeding probability  $P(EDP > z | \Gamma)$  can be obtained. Combining exceeding probability and scenario rate, EDP hazard of MIDR is calculated using Equation (6) and

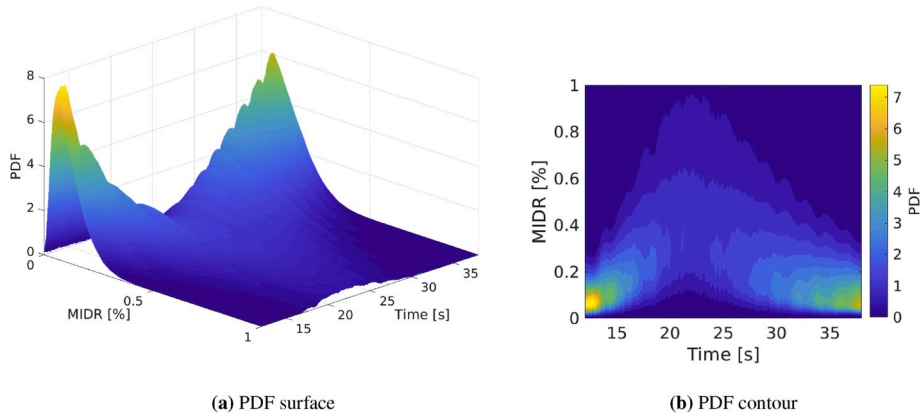


Fig. 12. Time evolving probability density function (PDF) of MIDR for frame structure.

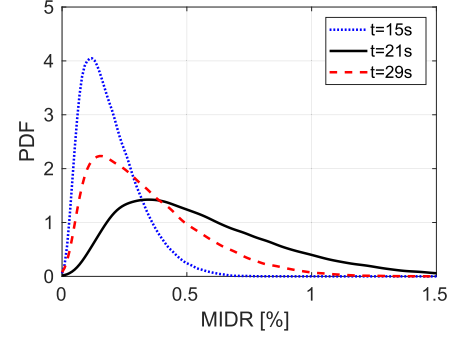


Fig. 13. PDF of MIDR at different times:  $t = 15s, 21s$  and  $29s$ .

is shown in Fig. 14(b).

It can be seen that the demand of MIDR is dominantly controlled by lower floors, e.g., the 1st and 3rd floor.

In addition to PDFs of MIDR, PDFs of PFA for different floors and the whole frame structure are developed and shown in Fig. 15(a). The distributions of PFA of the 1st, 3rd and 6th floor are close to each other, while the PFA of the top floor shows larger mean and variability. The PFA distribution of the top floor is very close to that of the whole structure, which indicates the top floor tends to experience the maximum acceleration. EDP hazard of PFA is shown in Fig. 15 (b). The demand of PFA is dominantly controlled by the top floor.

By assuming that damage measure (DM) is a step function of EDP, seismic risk for damage states using different levels of MIDR and PFA exceedance can be directly determined from the EDP hazard curve. As shown in Table 6, seismic risk for  $MIDR > 1\%$  is  $3.83 \times 10^{-3}$  and the risk for  $PFA > 1m/s^2$  is  $1.92 \times 10^{-3}$ .

As noted earlier, complete probabilistic structural response, including both marginal distribution and correlation information, is contained in PC coefficients, any other EDP or other DM defined on multiple EDPs can also be developed with little additional effort. Fig. 16 shows the 2D joint PDF,  $f(MIDR, PFA | \Gamma)$  of two EDPs, MIDR and PFA, evaluated from the PC-based surrogate model of probabilistic structure response.

It can be observed that in this case MIDR and PFA are positively correlated. The correlation coefficient is 0.64.

For damage measure (DM) defined on multiple EDPs, for example,  $DM : \{MIDR > z_1 \vee PFA > z_2\}$ , seismic risk can be evaluated as:

$$\lambda(MIDR > z_1 \vee PFA > z_2) = \bar{\lambda} \int_{\mathcal{D}} f(MIDR, PFA | \Gamma) d\mathcal{D} \quad (63)$$

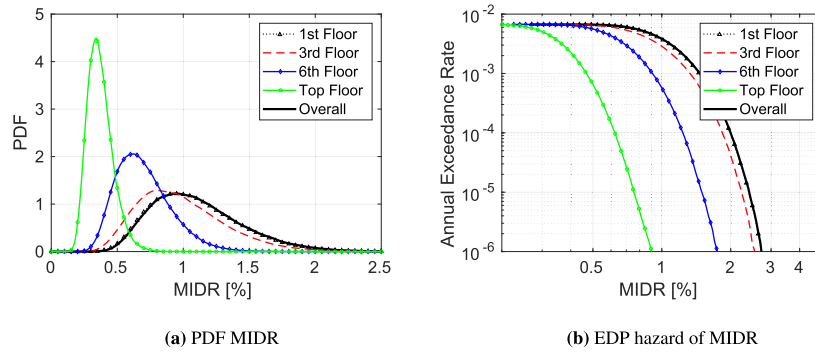


Fig. 14. PDF and annual exceedance rate of MIDR between different story over the whole loading history.

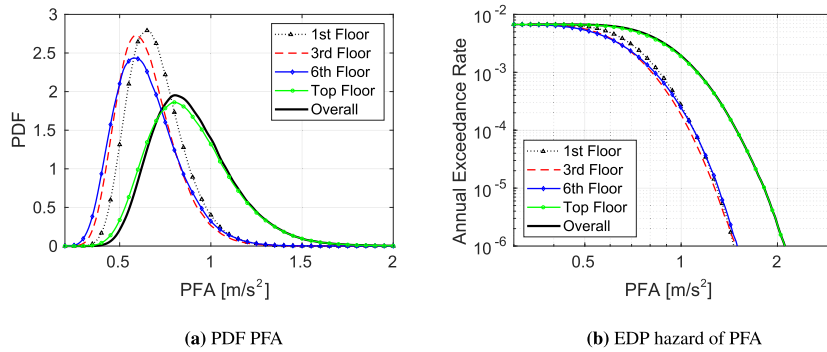


Fig. 15. PDF and annual exceedance rate of PFA of different stories and the whole frame structure.

Table 6

Seismic risk of damage state for different levels of MIDR and PFA exceedance.

MIDR > 0.5%	MIDR > 1%	MIDR > 2%	PFA > 0.5m/s <sup>2</sup>	PFA > 1m/s <sup>2</sup>	PFA > 1.5m/s <sup>2</sup>
$6.66 \times 10^{-3}$	$3.83 \times 10^{-3}$	$9.97 \times 10^{-5}$	$6.65 \times 10^{-3}$	$1.92 \times 10^{-3}$	$9.45 \times 10^{-5}$

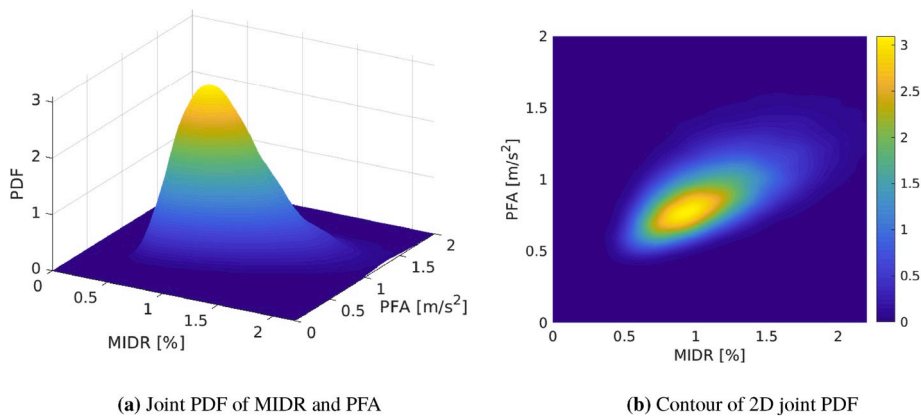


Fig. 16. 2D joint PDF of MIDR and PFA of the whole shear frame structure.

where  $\bar{\lambda}$  is the annual occurrence rate of seismic scenario that would induce ground motion population  $\Gamma$ , while  $\mathcal{S}$  is the integral domain  $(MIDR, PFA) \in [z_1, +\infty] \cup [z_2, +\infty]$  according to the definition of damage measure.

Using such approach, seismic risk for damage state  $DM$  defined for either MIDR greater than 1% or PFA greater than  $1m/s^2$  (i.e.,

$DM : \{MIDR > 1\% \vee PFA > 1m/s^2\}$ ), can be calculated as  $4.20 \times 10^{-3}$ , while the risk for damage state defined for both MIDR greater than 1% and PFA greater than  $1m/s^2$  (i.e.,  $DM : \{MIDR > 1\% \wedge PFA > 1m/s^2\}$ ) is 60% less, equal to  $1.71 \times 10^{-3}$ . Both of these risk values based on joint EDPs are rather different from the ones calculated using single EDP.

#### 4. Conclusions

A time domain intrusive probabilistic seismic risk analysis framework for performance based earthquake engineering was described in some detail. Methodology to simulate non-stationary stochastic seismic motions was presented. The presented methodology is directly compatible with state-of-the-art seismic source characterization. Different source, path and site factors are explicitly accounted for in the stochastic modeling of Fourier amplitude spectrum and Fourier phase derivative. Both uncertain seismic motions and uncertain structural parameters are characterized as random process/field and represented with Hermite polynomial chaos (PC) Karhunen-Loève (KL) expansion. Direct polynomial chaos based Galerkin intrusive modeling of 1D elastic-plastic response was formulated and applied to simulate the uncertain hysteretic behavior of restoring force versus inter-story drift for shear frame structure. Formulations for random stiffness polynomial chaos coefficients were derived and incorporated into stochastic Galerkin elastic-plastic finite element method.

Using developed stochastic elastic-plastic finite element method, probabilistic dynamic response of uncertain structural system driven by uncertain motions is intrusively solved. Following that, seismic risk for damage measure defined on single or multiple engineering demand parameter(s) was calculated. The proposed framework is illustrated within seismic risk analysis of an eight-story shear frame structure excited by uncertain strike-slip fault earthquakes.

#### Declaration of competing interest

Non-financial interest in the subject matter or materials discussed in this manuscript.

#### Acknowledgements

Presented research was primarily funded from the private sources, from the University of California and in small part the US-DOE.

#### Appendix A. Supplementary data

Supplementary data to this article can be found online at <https://doi.org/10.1016/j.soildyn.2020.106201>.

#### References

- Cornell CA. Progress and challenges in seismic performance assessment". PEER newsletter. 2000. <https://apps.peer.berkeley.edu/news/2000spring/performance.html>. [Accessed 1 August 2018].
- Gregor N, Abrahamson NA, Atkinson GM, Boore DM, Bozorgnia Y, Campbell KW, et al. Comparison of NGA-west2 GMPEs. *Earthq Spectra* 2014;30(3):1179–97.
- Stafford PJ, Bommer JJ. Theoretical consistency of common record selection strategies in performance-based earthquake engineering. In: *Advances in performance-based earthquake engineering*. Springer; 2010. p. 49–58.
- Iervolino I, De Luca F, Cosenza E. Spectral shape-based assessment of SDOF nonlinear response to real, adjusted and artificial accelerograms. *Eng Struct* 2010;32(9):2776–92.
- Huang Y-N, Whittaker AS, Luco N, Hamburger RO. Scaling earthquake ground motions for performance-based assessment of buildings. *J Struct Eng* 2009;137(3):311–21.
- Grigoriu M. Do seismic intensity measures (ims) measure up? *Probabilist Eng Mech* 2016;46:80–93.
- Davoodi M, Jafari M, Hadiani N. Seismic response of embankment dams under near-fault and far-field ground motion excitation. *Eng Geol* 2013;158:66–76.
- Baker JW. Probabilistic structural response assessment using vector-valued intensity measures. *Earthq Eng Struct Dynam* 2007;36(13):1861–83.
- Brune JN. Tectonic stress and the spectra of seismic shear waves from earthquakes. *J Geophys Res* 1970;75(26):4997–5009.
- Boore DM. Stochastic simulation of high-frequency ground motions based on seismological models of the radiated spectra. *Bull Seismol Soc Am* 1983;73(6A):1865–94.
- Boore DM. Simulation of ground motion using the stochastic method. *Pure Appl Geophys* 2003;160:635–76.
- Boore DM, Thompson EM. Revisions to some parameters used in stochastic-method simulations of ground motion. *Bull Seismol Soc Am* 2015;105(2A):1029–41.
- Stafford PJ. Interfrequency correlations among fourier spectral ordinates and implications for stochastic ground-motion simulation. *Bull Seismol Soc Am* 2017;107(6):2774–91.
- Bayless J, Abrahamson NA. An empirical model for the interfrequency correlation of epsilon for fourier amplitude spectra. *Bull Seismol Soc Am* 2019;109(3):1058–70.
- Baglio MG. Stochastic ground motion method combining a fourier amplitude spectrum model from a response spectrum with application of phase derivatives distribution prediction. Ph.D. thesis. Politecnico di Torino; 2017.
- Vamvatsikos D, Cornell CA. Incremental dynamic analysis. *Earthq Eng Struct Dynam* 2002;31(3):491–514.
- Graves RW, Pitarka A. Broadband ground-motion simulation using a hybrid approach. *Bull Seismol Soc Am* 2010;100(5A):2095–123.
- Maechling P, Deelman E, Zhao L, Graves R, Mehta G, Gupta N, et al. SCEC cybershake workflows—automating probabilistic seismic hazard analysis calculations. *Workflows for e-Science*, Springer; 2007. p. 143–63.
- Graves R, Jordan T, Callaghan S, Deelman E, Field E, Juve G, et al. Cybershake: a physics-based seismic hazard model for southern California. *Pure Appl Geophys* 2011;168(3):367–81.
- Jeremić B, Sett K, Kavvas ML. Probabilistic elasto-plasticity: formulation in 1D. *Acta Geotechnica* 2007;2(3):197–210.
- Sett K, Jeremić B, Kavvas ML. Probabilistic elasto-plasticity: solution and verification in 1D. *Acta Geotechnica* 2007;2(3):211–20.
- Sett K, Jeremić B, Kavvas ML. Stochastic elastic-plastic finite elements. *Comput Methods Appl Mech Eng* 2011;200(9–12):997–1007.
- Karapiperis K, Sett K, Kavvas ML, Jeremić B. Fokker-planck linearization for non-Gaussian stochastic elastoplastic finite elements. *Comput Methods Appl Mech Eng* 2016;307:451–69.
- Wang F, Sett K. Time-domain stochastic finite element simulation of uncertain seismic wave propagation through uncertain heterogeneous solids. *Soil Dynam Earthq Eng* 2016;88:369–85.
- Wang F, Sett K. Time domain stochastic finite element simulation towards probabilistic seismic soil-structure interaction analysis. *Soil Dynam Earthq Eng* 2019;116:460–75.
- Xiu D. Numerical methods for stochastic computations. Princeton University Press; 2010.
- Elman HC, Miller CW, Phipps ET, Tuminaro RS. Assessment of collocation and Galerkin approaches to linear diffusion equations with random data. *Int J Uncertain Quantification* 2011;1(1).
- Sakamoto S, Ghanem R. Polynomial chaos decomposition for the simulation of non-Gaussian nonstationary stochastic processes. *J Eng Mech* 2002;128(2):190–201.
- Zheng Z, Dai H. Simulation of multi-dimensional random fields by Karhunen-Loève expansion. *Comput Methods Appl Mech Eng* 2017;324:221–47.
- Field EH, Jordan TH, Page MT, Milner KR, Shaw BE, Dawson TE, et al. A synoptic view of the third uniform California earthquake rupture forecast (UCERF3). *Seismol Res Lett* 2017;88(5):1259–67.
- McGuire RK. Seismic hazard and risk analysis. Earthquake Engineering Research Institute; 2004.
- Youngs RR, Coppersmith KJ. Implications of fault slip rates and earthquake recurrence models to probabilistic seismic hazard estimates. *Bull Seismol Soc Am* 1985;75(4):939–64.
- Leonard M. Earthquake fault scaling: self-consistent relating of rupture length, width, average displacement, and moment release. *Bull Seismol Soc Am* 2010;100(5A):1971–88.
- Hale C, Abrahamson N, Bozorgnia Y. Probabilistic seismic hazard analysis code verification. In: Report No. PEER 2018/03, Pacific earthquake engineering research center. Berkeley: Headquarters at the University of California; 2018.
- Coppersmith KJ, Salomone LA, Fuller CW, Glaser LL, Hanson KL, Hartleb RD, et al. Central and eastern United States (CEUS) seismic source characterization (SSC) for nuclear facilities. United States: Electric Power Research Institute; 2012. Report no.
- Moschetti MP, Powers PM, Petersen MD, Boyd OS, Chen R, Field EH, et al. Seismic source characterization for the 2014 update of the US national seismic hazard model. *Earthq Spectra* 2015;31(S1):S31–57.
- Musson R. On the nature of logic trees in probabilistic seismic hazard assessment. *Earthq Spectra* 2012;28(3):1291–6.
- Boore DM. Phase derivatives and simulation of strong ground motions. *Bull Seismol Soc Am* 2003;93(3):1132–43.
- Bora SS, Scherbaum F, Kuehn N, Stafford P, Edwards B. Development of a response spectral ground-motion prediction equation (GMPE) for seismic-hazard analysis from empirical fourier spectral and duration models. *Bull Seismol Soc Am* 2015;105(4):2192–218.
- Montaldo V, Kiremidjian A, Thraínsson H, Zonno G. Simulation of the fourier phase spectrum for the generation of synthetic accelerograms. *J Earthq Eng* 2003;7:427–45. 03.
- Ohsaki Y. On the significance of phase content in earthquake ground motions. *Earthq Eng Struct Dynam* 1979;7(5):427–39.
- Thraínsson H, Kiremidjian AS. Simulation of digital earthquake accelerograms using the inverse discrete fourier transform. *Earthq Eng Struct Dynam* 2002;31(12):2023–48.
- Atkinson GM, Boore DM. Ground-motion relations for eastern north America. *Bull Seismol Soc Am* 1995;85(1):17–30.
- Boore DM. SMSIM: fortran programs for simulating ground motions from earthquakes. Citeseer; 2005. Version 2.3.

- [45] Bora SS, Cotton F, Scherbaum F. NGA-West2 empirical fourier and duration models to generate adjustable response spectra. *Earthq Spectra* 2018;2.
- [46] Xu J, Feng D-C. Stochastic dynamic response analysis and reliability assessment of non-linear structures under fully non-stationary ground motions. *Struct Saf* 2019; 79:94–106.
- [47] Lubliner J. *Plasticity theory*. New York: Macmillan Publishing Company; 1990.
- [48] Newmark NM. A method of computation for structural dynamics. *ASCE J Eng Mechan Div* 1959;85:67–94.
- [49] Hilber HM, Hughes TJR, Taylor RL. Improved numerical dissipation for time integration algorithms in structural dynamics. *Earthquake Eng Struct Dyna* 1977;5 (3):283–92.
- [50] Sett K, Unutmaz B, Önder Çetin K, Koprivica S, Jeremić B. Soil uncertainty and its influence on simulated  $G/G_{max}$  and damping behavior. *ASCE J Geotech Geoenviron Eng* 2011;137(3):218–26. 10.1061/(ASCE)GT.1943-5606.0000420 (July 29, 2010).
- [51] Arnst M, Ghanem R. A variational-inequality approach to stochastic boundary value problems with inequality constraints and its application to contact and elastoplasticity. *Int J Numer Methods Eng* 2012;89(13):1665–90.
- [52] Rosić BV, Matthies HG. Variational theory and computations in stochastic plasticity. *Arch Comput Methods Eng* 2014:1–53.
- [53] Armstrong P, Frederick C. A mathematical representation of the multiaxial Bauschinger effect. C.E.G.B; 1966. Technical Report RD/B/N/731.
- [54] Dettmer W, Reese S. On the theoretical and numerical modelling of Armstrong-Frederick kinematic hardening in the finite strain regime. *Comput Methods Appl Mech Eng* 2004;193(1–2):87–116.
- [55] Li J, Chen J-B. The probability density evolution method for dynamic response analysis of non-linear stochastic structures. *Int J Numer Methods Eng* 2006;65(6): 882–903.
- [56] Mitseas IP, Kougioumtzoglou IA, Giaralis A, Beer M. A novel stochastic linearization framework for seismic demand estimation of hysteretic mdf systems subject to linear response spectra. *Struct Saf* 2018;72:84–98.
- [57] Papazafeiropoulos G, Plevris V, Papadrakakis M. A new energy-based structural design optimization concept under seismic actions. *Front Built Environ* 2017;3:44.
- [58] Sudret B. Global sensitivity analysis using polynomial chaos expansions. *Reliab Eng Syst Saf* 2008;93(7):964–79.
- [59] Miranda E, Taghavi S. Approximate floor acceleration demands in multistory buildings. i: Formulation. *J Struct Eng* 2005;131(2):203–11.
- [60] Miranda E, Akkar S. Generalized interstory drift spectrum. *J Struct Eng* 2006;132 (6):840–52.
- [61] Bayless J, Abrahamson NA. Evaluation of the interperiod correlation of ground-motion simulations. *Bull Seismol Soc Am* 2018;108(6):3413–30.